Diffusion Kinetics of HCl Hydrates in Ice Measured Using Infrared Laser Resonant Desorption Depth-Profiling

Frank E. Livingston and Steven M. George*

Department of Chemistry and Biochemistry, University of Colorado, Boulder, Colorado 80309-0215

Received: December 6, 2000; In Final Form: March 8, 2001

The diffusion kinetics of HCl hydrates in ice were measured using a new infrared laser resonant desorption (LRD) depth-profiling technique. This LRD technique permits quantitative depth-profiling and real time diffusion measurements in ice with submicron spatial resolution and high sensitivity. The diffusion coefficients of HCl hydrates ranged from $D = 2.0(\pm 0.6) \times 10^{-13}$ cm^2/s at $T = 169.0$ K to $D = 1.1(\pm 0.2) \times 10^{-10}$ cm^2/s at $T = 194.9$ K. Arrhenius analysis of the diffusion rates yielded a diffusion activation energy of $E_A = 15.3 \pm 1.0$ kcal/mol and a diffusion preexponential of $D_o = 1.5 \times 10^{7\pm0.2}$ cm^2/s. The diffusion coefficients were independent of the total diffusion time and the initial HCl exposure conditions used to prepare the HCl hydrates. The HCl diffusion rates were comparable to H_2O diffusion rates in pure ice and HCl-dosed ice multilayers. This similarity between the HCl and H_2O diffusion rates suggests that HCl hydrate diffusion in ice may be dependent on the diffusion of H_2O vacancies.

I. Introduction

Diffusion in ice can impact processes occurring on glacial and polar ice sheets[1−4] and heterogeneous chemistry on cirrus and polar stratospheric clouds.[5−7] Ice cores provide critical insight into the past chemical composition of the Earth's atmosphere.[1,2] Postdepositional migration can influence the interpretation and preservation of this paleoclimatic information.[1,4] Diffusion of species into ice can also impact heterogeneous atmospheric chemistry because ice is known to produce active chlorine species that can deplete ozone and act as a reservoir for various atmospheric species.[7−11] Despite the importance of diffusion in ice, very few measurements have been conducted because of experimental difficulties.

The solubility and diffusion of hydrogen chloride (HCl) in ice have received attention because HCl plays a significant role in controlling the acidity of the atmosphere.[12] The interaction of HCl with ice is also important in the heterogeneous chemistry of the upper troposphere[13−17] and polar stratosphere.[6,7,10,11] HCl diffusion in ice can affect the reaction kinetics of chlorine activation on ice clouds and influence the ability of ice particles to sequester HCl. HCl diffusion can also control the extent of HCl removal from the gas phase via sedimentation and influence the dechlorination of the polar stratosphere.[18]

The diffusion kinetics of HCl in ice have been examined by numerous direct and indirect experimental methods.[1,8,12,19−25] Unfortunately, the HCl diffusion results vary widely from $D \approx 10^{-5}$ cm^2/s to $D \approx 10^{-13}$ cm^2/s at a temperature of 185 K that is typical for the polar stratosphere. The large discrepancies in the HCl diffusion results may be attributable to the wide variety of experimental techniques and ice substrates that have been employed for the HCl diffusion studies.[1,8,12,19−25] In particular, the HCl concentrations, various spatial resolutions and detection sensitivities, and varying ice growth conditions and ice film morphologies have likely contributed to the broad range of measured HCl diffusion rates.

The first study measuring HCl diffusion and solubility utilized radioactive tracer and liquid scintillation spectrometric methods to monitor $H^{36}Cl$ diffusion and solubility in single-crystal ice samples.[21] These HCl tracer measurements yielded HCl diffusion coefficients ranging from $D = 2.2 \times 10^{-8}$ cm^2/s at $T = 255$ K to $D = 1.6 \times 10^{-7}$ cm^2/s at $T = 269$ K. More recently, spectroscopic methods have been employed to monitor the HCl concentration gradient in polycrystalline ice exposed to high HCl partial pressures ranging from 0.01 to 1 Torr.[8] These spectroscopic results imply rapid HCl diffusion in ice with an apparent HCl diffusion coefficient of $D \approx 10^{-5}$ cm^2/s at $T = 185$ K.

Scanning electron microscopy (SEM) and X-ray analysis have also been employed to study HCl incorporation and movement in frozen HCl−H_2O solutions.[26] These experiments revealed that HCl solubilities and mobilities in ice crystals are very small and yielded an upper limit on the HCl diffusion coefficient of $D < 10^{-13}$ cm^2/s at 253 K. Extensive studies on the diffusion coefficients and equilibrium solubilities of HCl in ice have also been performed using microtome analysis and ion chromatography.[12,19,20] HCl diffusion coefficients were measured that ranged from $D = 4.0 \times 10^{-12}$ cm^2/s at $T = 238$ K to $D = 7.2 \times 10^{-12}$ cm^2/s at $T = 265$ K.

With the hope of resolving the earlier discrepancies, the present study investigated HCl diffusion rates in ice using a novel infrared laser resonant desorption (LRD) depth-profiling technique. This new LRD technique was described in detail in previous publications.[27,28] In brief, HCl depth-profiling and diffusion measurements in H_2O ice films were accomplished using LRD to desorb thin ice layers consecutively from the surface of ice. The LRD is performed using an Er:YAG rotary Q-switched laser with an output wavelength of $\lambda = 2.94$ μm and a pulse duration of ~100 ns. The Er:YAG laser radiation excites the O−H stretching vibration in the H_2O molecules and the subsequent resonant heating induces H_2O desorption from the ice surface. Sequential laser pulses can depth-profile into the ice sample and a quadrupole mass spectrometer can identify species in each thin ice layer.

* To whom correspondence should be addressed. Fax: 303-492-5894. E-mail: georges@spot.Colorado.edu.

10.1021/jp0043773 CCC: $20.00
Published on Web 05/09/2001

Measurements of HCl diffusion in crystalline H_2O ice films were performed by monitoring the spatial relaxation of a HCl hydrate interlayer encapsulated in a H_2O/HCl/H_2O sandwich structure versus time at constant temperature.[27] The measured HCl coverage distributions at successive diffusion times were used to derive the diffusion coefficients for the HCl hydrates in ice over the temperature range from $T = 169.0-194.9$ K. These results demonstrate the ability of the LRD technique to perform quantitative measurements of diffusion kinetics in ice. Comparison between these HCl diffusion kinetics and previously measured H_2O diffusion kinetics also provides insight into the mechanism of HCl hydrate diffusion in ice.

II. Experimental Section

A. Laser Resonant Desorption (LRD) Depth-Profiling. Earlier publications provided a detailed description of the experimental setup and rotary Q-switched Er:YAG laser.[27,29,30] The LRD experiments were conducted in an ultrahigh vacuum (UHV) chamber located on a vibrationally isolated optical table. The UHV apparatus was pumped by a 200 L/s ion pump, a titanium sublimation pump and liquid nitrogen cooled cryopanels. Typical baseline pressures in the UHV chamber were $<2.0 \times 10^{-10}$ Torr. The UHV apparatus was equipped with a low energy electron diffraction (LEED) spectrometer and Auger electron spectrometer (AES) with a single-pass cylindrical mirror analyzer (CMA) for surface structure and surface cleanliness measurements.

Crystalline ice films were grown on a single-crystal Ru(001) metal substrate with a diameter of 8 mm and a thickness of 1 mm. The excellent lattice match between Ru(001) and hexagonal ice promotes the growth of crystalline ice films.[29] The Ru(001) substrate was mounted on a copper sample holder attached to a liquid nitrogen cooled cryostat.[31] H_2O deposition was accomplished using a glass multichannel capillary array doser positioned approximately 1 cm from the Ru(001) substrate surface. Prior to ice film growth, trace contaminants were removed from the Ru(001) substrate surface using established cleaning procedures.[32]

The measurements of HCl hydrate diffusion in crystalline ice were performed using the infrared LRD depth-profiling technique.[27,28] LRD was accomplished using a Er:YAG TEM_{oo} Q-switched laser (LaserSight Technologies, Inc., Model 1-2-3) with an output wavelength of λ=2.94 μm and a pulse duration of ~100 ns. A newly designed close-coupled circular diffuse $BaSO_4$ reflector cavity (Shiva Laser Systems, Inc.) was implemented to achieve high laser output energies and enhanced pulse-to-pulse stability.[27] The Er:YAG laser radiation resonantly pumps the O−H stretching vibration in the H_2O molecules in the ice lattice. The incident laser energy is rapidly thermalized and induces desorption in the near surface region of the ice film.[27]

The imaginary component of the refractive index is $k(\lambda) \approx 0.3$ at $\lambda = 2.94$ μm and corresponds to a theoretical optical penetration depth $p = \lambda/4\pi k(\lambda) \approx 0.8$ μm in crystalline ice.[33] The small optical penetration depth at $\lambda = 2.94$ μm and short pulse duration achievable with the Er:YAG Q-switched laser help to ensure that the laser resonant heating remains localized on the time scale of the laser pulse. This localization minimizes thermal damage to the surrounding ice multilayer. The localization of the laser heating to <1 μm also permits depth-profiling in ice with submicron spatial resolution and high sensitivity.

Figure 1 shows a schematic representation of the LRD depth-profiling method. A series of Er:YAG laser pulses are used to desorb iteratively thin layer sections of the ice film. The incident

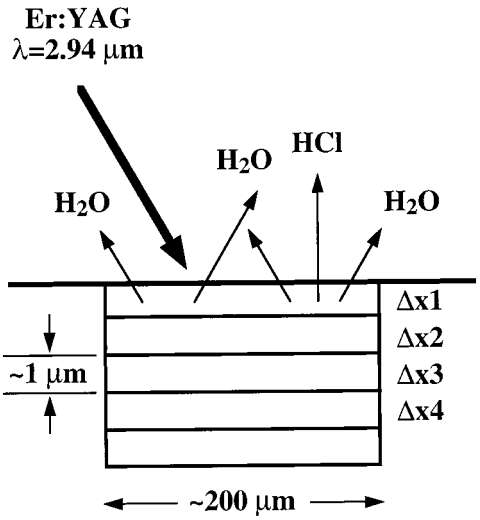

Figure 1. Representation of the laser resonant desorption (LRD) depth-profiling experiment. A series of Er:YAG laser pulses are used to desorb iteratively thin layer sections of the ice film. The LRD depth is near the optical penetration depth of ~1 μm.

laser energy can be adjusted to achieve the desired probe depth in the ice film. Previous LRD depth-profiling studies have demonstrated that H_2O desorption depths ranging from 0.20 μm at $E = 0.40$ mJ/pulse to 0.64 μm at $E = 0.74$ mJ/pulse can be readily obtained by adjusting the Er:YAG laser pulse energy.[27]

The desorbed species are mass analyzed with high sensitivity using an Extrel C50 quadrupole mass spectrometer with line-of-sight to the ionizer. Consecutive laser pulses desorb deeper into the ice bulk. The quadrupole mass spectrometer signals are recorded for each Δx sublayer. These measurements permit the spatial concentration profile of the diffusing species to be determined versus distance into the ice bulk.

Laser pulses were incident at an angle of 54° with respect to the surface normal. The pulses were focused using an uncoated CaF_2 lens with a focal length of 760 mm. This optical geometry produced elliptical desorption areas with typical dimensions of ~175 μm × ~225 μm as measured by spatial autocorrelation methods.[34] Glass microscope slides were used to attenuate the laser pulses to the desired energy. A UV grade sapphire viewport was employed to transmit the Er:YAG laser radiation into the UHV chamber. The laser beam was translated across the ice film using mirrors mounted on piezoelectric translators. The location of the laser beam on the ice film surface could be adjusted with a precision of ±0.5 μm.

The ice film thickness was determined using optical interferometry during isothermal desorption of the ice film following LRD depth-profile analysis.[35] A helium neon laser with an output wavelength of $\lambda = 0.5940$ μm and energy of 5 mW output was used to perform the optical interference measurements. The ice film thickness could be determined with an accuracy of ±0.05 μm.

B. LRD Measurements of HCl Hydrate Diffusion. Diffusion measurements were performed by monitoring the spatial HCl concentration versus time using LRD probing as depicted in Figure 2. A laminated HCl sandwich structure was prepared by initially growing an ice multilayer on the single-crystal Ru(001) metal substrate using the capillary array doser. The H_2O sample (HPLC Grade, Fisher Scientific) was purified by several freeze−pump−thaw cycles with liquid nitrogen prior to use. The bottom ice film layers were grown at temperatures

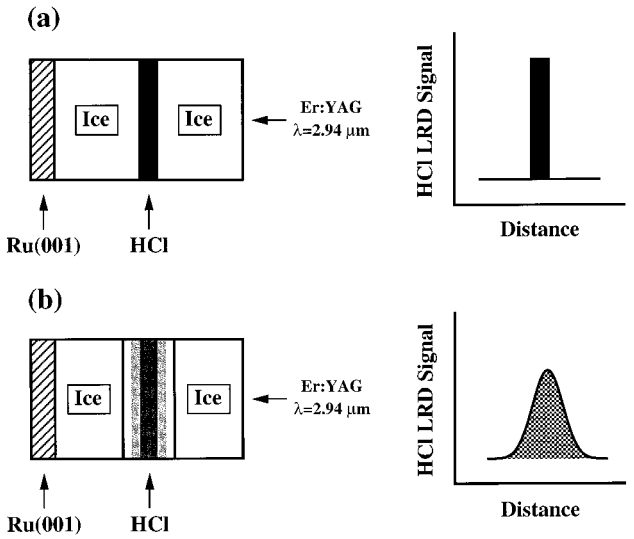

Figure 2. Representation of the LRD depth-profiling experiment on ice laminate structures. (a) The Er:YAG laser beam depth-profiles into the ice laminate and measures the initial HCl spatial coverage profile. (b) A second LRD depth-profile observes the spatial relaxation of the initial HCl coverage gradient after HCl diffusion.

ranging from $T = 100-160$ K and subsequently annealed to ensure crystallinity.[29]

Gaseous hydrogen chloride (HCl, >99% anhydrous grade, Aldrich Chemical Co., Inc.) was then deposited on top of this ice multilayer using a separate glass multichannel capillary array doser. Low temperatures were employed for HCl deposition to avoid possible HCl adlayer desorption or preliminary HCl diffusion. Typical HCl exposures used to prepare the HCl interlayer were $\sim 2.4 \times 10^{-4}$ Torr s at an ice film temperature of ~140 K. Previous studies have shown that HCl exposures ranging from $\sim 1 \times 10^{-4}$ Torr s to $\sim 5 \times 10^{-4}$ Torr s at 140 K yield a HCl trihydrate phase with a localized stoichiometry of $HCl{:}3H_2O$.[36]

The H_2O LRD signals and calibrated HCl LRD signals were consistent with an initial HCl trihydrate interlayer with a thickness of ~0.1 μm. The number of H_2O molecules desorbed per laser pulse was calculated from the LRD desorption volume and the density of ice. The LRD desorption volume was determined directly from the measured LRD desorption area and desorption depth. The HCl LRD signal was then calibrated relative to the H_2O LRD signal by correcting for the relative ionization efficiencies and mass spectrometer fragmentation patterns. For H_2O, the fragmentation pattern was derived by measuring the intensity of $^{16}O^+$ ($m/e = 16$), $^{16}OH^+$ ($m/e = 17$) and $H_2{}^{16}O^+$ ($m/e = 18$). The H_2O fragmentation pattern accounted for contributions from the protonated monomer water cluster at $H^+[H_2{}^{16}O]$, ($m/e = 19$). For HCl, the cracking distribution was determined by measuring the intensity of $^{35}Cl^+$ ($m/e = 35$), $^{37}Cl^+$ ($m/e = 37$), $H^{35}Cl^+$ ($m/e = 36$) and $H^{37}Cl^+$ ($m/e = 38$). The HCl calibration also accounted for contributions from the protonated dimer water cluster at $H^+[H_2{}^{16}O]_2$, ($m/e = 37$).

The ice laminate sandwich structure was completed by growing an additional ice layer on top of the HCl adlayer section at $T \leq 140$ K to encapsulate the HCl. The structure of the top ice layer is likely amorphous at $T \leq 140$ K. However, the top ice layer will crystallize at the high temperatures ($T > 168$ K) employed in the LRD diffusion measurements.[29] The Er:YAG laser was then used to depth-profile into the ice laminate structure and measure the spatial HCl profile versus diffusion time. Prior to diffusion, the HCl should remain well localized in the ice laminate structure. Consequently, the initial LRD depth-profile at time $t = 0$ should resemble a top-hat profile as shown in Figure 2a.

The temperature of the ice laminate was then raised to the desired diffusion temperature for a fixed time interval. For diffusion temperatures ≥185 K, H_2O desorption rates are ≥0.46 μm/min[35,37] and an H_2O overpressure is needed to maintain a nearly constant top ice multilayer thickness during the diffusion experiment. The H_2O overpressure was supplied using the glass multichannel capillary array doser. An H_2O overpressure was not required for the LRD diffusion measurements at $T < 185$ K. After the HCl hydrate was allowed to diffuse, the ice multilayer was cooled rapidly to terminate further diffusion and a second LRD depth-profile was obtained using the Er:YAG laser. Diffusion of the HCl species will result in the spatial relaxation of the initial top-hat HCl gradient as illustrated in Figure 2b.

C. Computer Modeling of HCl Diffusion. Diffusion coefficients for the migration of HCl hydrates in ice were extracted by fitting the experimental data to computer simulations. The HCl diffusion process can be described as the spatial relaxation of an extended initial distribution in an infinite medium using the following relationship derived from Fick's Law:[38]

$$\frac{C(x,t)}{C_o(x,0)} = 0.5\left[\mathrm{erf}\left(\frac{h-x}{2\sqrt{Dt}}\right) + \mathrm{erf}\left(\frac{h+x}{2\sqrt{Dt}}\right)\right] \qquad (1)$$

In this equation, D is the diffusion coefficient, $\pm h$ (or $2h$) is the initial interlayer width of the diffusing species, and erf is the error function. $C_o(x,0)$ represents the initial concentration of the diffusing species at time $t = 0$ and distance x. Similarly, $C(x,t)$ corresponds to the concentration of the diffusing species at a distance x after a diffusion time t. $C(x,t)$ can be obtained from the HCl LRD depth-profile signals after the HCl has diffused distances greater than the H_2O desorption depth during LRD.

$C_o(x,0)$ and h are not directly measurable if the H_2O desorption depth during LRD is greater than the initial interlayer width. However, values for the initial concentration, $C_o(x,0)$, and the initial interlayer width, $2h$, must meet two specific criteria. The integrated LRD signal, S, under each measured spatial concentration profile must remain constant to conserve mass. Consequently, the $C_o(x,0)$ and h values must meet the requirement that $S = k2hAC_o(x,0)$, where k is a constant and A is the elliptical LRD area. The initial interlayer width, $2h$, must also be consistent with the H_2O desorption depth during LRD. If the initial interlayer is desorbed and detected in a single laser pulse at time $t = 0$, then the initial interlayer width can not exceed the desorption depth.

The simulated concentration profiles are not very sensitive to the choice of the initial $C_o(x,0)$ and h values that obey the two specific criteria. Figure 3a shows the concentration profiles versus distance at time $t = 0$ for two different initial spatial distributions. The solid line in Figure 3a corresponds to an initial interlayer width $\pm h = 0.01$ μm and an initial concentration such that $kAC_o(x,0) = 10^4$ μm^{-1}. The dotted line represents a spatial distribution defined by $\pm h = 0.2$ μm and $kAC_o(x,0) = 500$ μm^{-1}. Note that the total signals under each profile are both $S = k2hAC_o(x,0) = 200$.

Figure 3b displays the simulated concentration profiles versus distance after the initial spatial distributions in Figure 3a have been allowed to relax according to eq 1 for $t = 120$ s using a diffusion coefficient of $D = 5.0 \times 10^{-11}$ cm^2/s. The simulated profiles in Figure 3b demonstrate that the resulting concentration

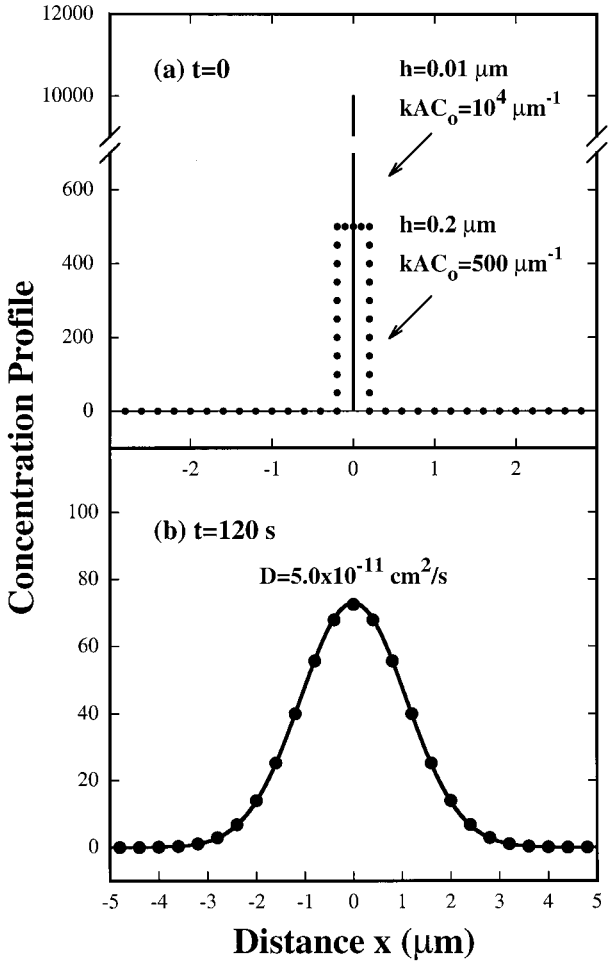

Figure 3. Simulated concentration profiles versus distance for two different initial spatial distributions (a) prior to diffusion at $t = 0$ and (b) after diffusional relaxation for $t = 120$ s. The initial interlayer widths of h=0.01 μm and 0.2 μm with kAC_o=10^4 μm^{-1} and 500 μm^{-1}, respectively, yield identical concentration profiles after $t = 120$s with $D = 5.0 \times 10^{-11}$ cm^2/s.

profiles that originated from markedly different initial profiles are indistinguishable after diffusional relaxation for $t = 120$ s. Similar results were obtained for diffusion coefficients ranging from $D \approx 1 \times 10^{-13}$ cm^2/s to $D \approx 1 \times 10^{-10}$ cm^2/s. However, as the diffusion coefficient is decreased, longer diffusion times are required to yield equivalent concentration profiles.

Simulated concentration profiles during the spatial relaxation of an initial top-hat distribution in an infinite medium are displayed in Figure 4. The simulations show the normalized concentration of the interlayer species as a function of distance for diffusion times ranging from 0 to 1500 s. The concentration profiles shown in Figure 4 were derived using eq 1 with an initial interlayer width of h=0.5 μm and a diffusion coefficient of $D = 1.0 \times 10^{-11}$ cm^2/s. Figure 4 shows that a diffusion coefficient of $D = 1.0 \times 10^{-11}$ cm^2/s would correspond to migration lengths of $\sim$0.5$-$3 μm after diffusion times of $t =$ 100$-$1500 s. Given the submicron desorption depths and diffusion times of several hours, LRD diffusion measurements can be performed for species that have diffusion coefficients as small as $D \approx 1 \times 10^{-13}$ cm^2/s.

III. Results

A. Diffusion of HCl Hydrates in Ice. The measured HCl LRD signals versus distance into an ice laminate structure at a low diffusion temperature of 169.8 K are shown in Figure 5.

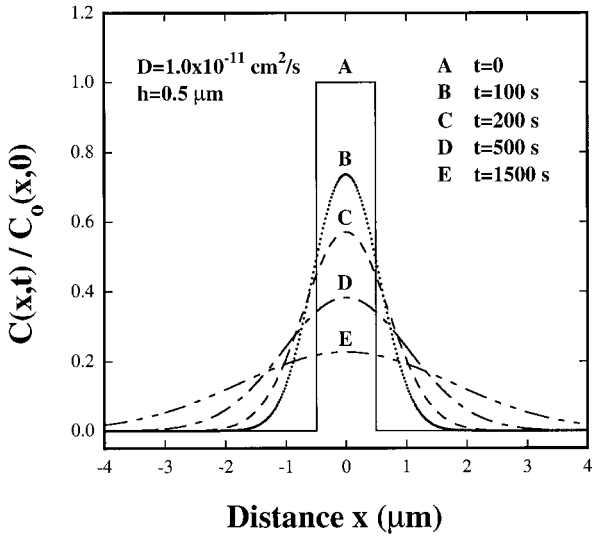

Figure 4. Normalized concentration profiles versus distance predicted for diffusional relaxation. The initial interlayer width was $\pm$h=0.5 μm and the diffusion coefficient was $D = 1.0 \times 10^{-11}$ cm^2/s.

The HCl in the ice film was detected by monitoring $^{35}Cl^+$ at $m/e = 35$. The thickness of the top and bottom ice layers was 5 μm. The experimental LRD results are denoted by the solid circles and the diffusion simulations from eq 1 are shown as the solid lines. Each data point represents the HCl signal derived from a single laser pulse and corresponds to a desorption depth of 0.5 μm at a laser pulse energy of $E = 0.60 \pm 0.01$ mJ.

The LRD depth-profiling results in Figure 5a show that the HCl hydrate interlayer at 110 K is initially well localized at $t = 0$. The HCl hydrate interlayer width is less than the desorption depth and all the HCl is desorbed in a single laser pulse. The temperature of the ice multilayer was then raised to $T = 169.8$ K for $t = 1800$ s. Subsequently, the ice multilayer was cooled rapidly to $\sim$110 K to terminate further HCl diffusion. The LRD results obtained after 1800 s at 169.8 K are shown in Figure 5b. The HCl coverage gradient has relaxed with HCl diffusion occurring over $\sim$0.5 μm.

Simulations of the spatial relaxation shown in Figure 5b using eq 1 yield a HCl diffusion coefficient of $D = 4.1(\pm 1.0) \times 10^{-13}$ cm^2/s at $T = 169.8$ K. This diffusion coefficient was obtained using $2h$ and kAC_o values ranging from 0.01 to 0.50 μm and $2.0 \times 10^4 - 400$ μm^{-1}, respectively. The LRD depth-profiling results obtained at $T = 169.8$ K for a diffusion time of $t =$ 5400 s are shown in Figure 5c. The HCl LRD results indicate that HCl migration has occurred over lengths of $\sim$1 μm. Similar simulations fit to the LRD data yield a diffusion coefficient of $D = 4.3(\pm 0.8) \times 10^{-13}$ cm^2/s.

The LRD results for a high-temperature HCl diffusion experiment at $T = 189.4$ K are shown in Figure 6. The thicknesses of the top and bottom H_2O ice multilayers were 7 μm and 10 μm, respectively. The incident laser pulse energy was $E = 0.61 \pm 0.02$ mJ and corresponds to a LRD desorption depth of $\sim$0.5 μm for each laser pulse. The LRD depth-profiling results measured prior to HCl diffusion at $t = 0$ are displayed in Figure 6a. These HCl LRD results show that the HCl hydrate interlayer remains well localized at $t = 0$ and $T = 110$ K.

The temperature of the ice sandwich structure was then raised to $T = 189.4$ K for $t = 120$ s. An H_2O overpressure was required during this HCl diffusion experiment because of the rapid H_2O desorption rate from ice films at these higher temperatures.[35,37] The ice film was then cooled rapidly to $\sim$110 K to prevent further HCl diffusion. The HCl LRD coverage profile measured

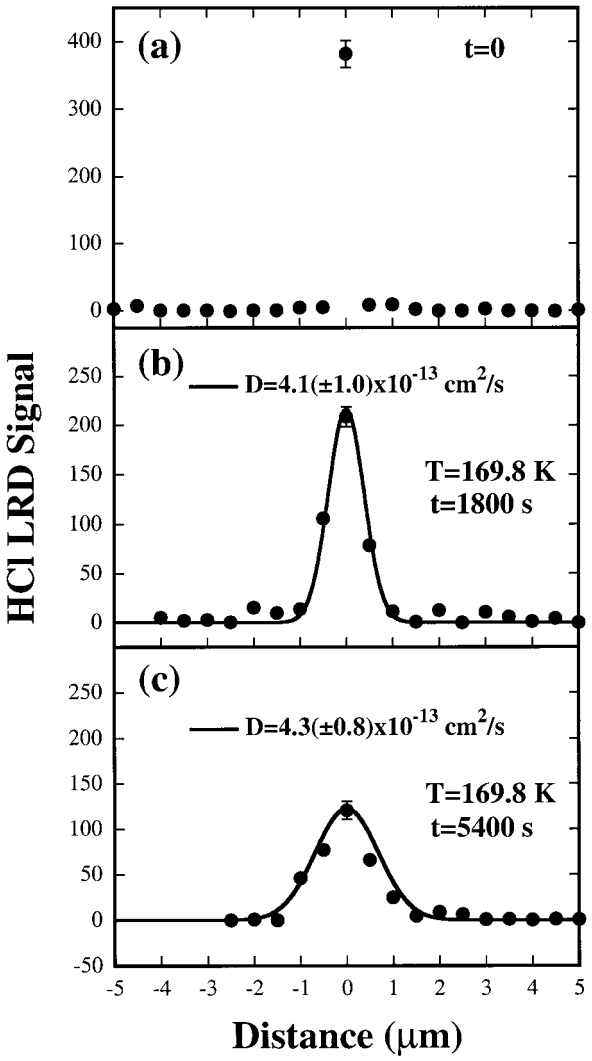

Figure 5. HCl LRD signals versus distance into the ice film measured using the Er:YAG laser with $E = 0.60 \pm 0.01$ mJ/pulse (a) at $t = 0$ s, (b) after diffusion at $T = 169.8$ K for $t = 1800$ s, and (c) after diffusion at $T = 169.8$ K for $t = 5400$ s. The thickness of the top and bottom ice multilayers was 5 μm. The experimental LRD results are represented by the solid circles and the Fick's Law diffusion simulations are shown as the solid lines.

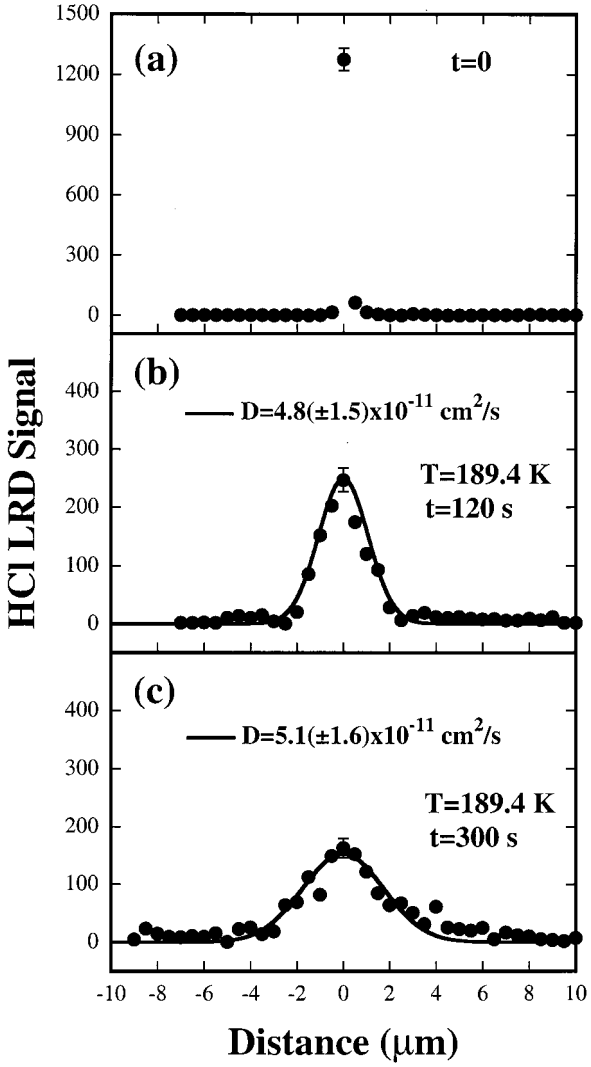

Figure 6. HCl LRD signals versus distance into the ice film measured using the Er:YAG laser with $E = 0.61 \pm 0.01$ mJ/pulse (a) at $t = 0$ s, (b) after diffusion at $T = 189.4$ K for $t = 120$ s, and (c) after diffusion at $T = 189.4$ K for $t = 300$ s. The thicknesses of the top and bottom ice multilayers were 7 μm and 10 μm, respectively.

at $t = 120$ s is shown in Figure 6b. These LRD results reveal that the HCl coverage gradient has relaxed considerably with HCl diffusion occurring over $\sim$2 μm. The solid line corresponding to the solid circles in Figure 6b represents a fit to the HCl LRD signals with $D = 4.8(\pm 1.5) \times 10^{-11}$ cm^2/s. This diffusion coefficient was derived utilizing 2h and kAC_o values ranging from 0.01 to 0.50 μm and $6.0 \times 10^4 - 1200$ μm^{-1}, respectively.

The LRD depth-profiling results obtained after diffusion at $T = 189.4$ K for $t = 300$ s are shown in Figure 6c. These HCl LRD results demonstrate that the HCl coverage gradient has relaxed further with HCl diffusion occurring over lengths of $\sim$4 μm. Similar diffusion simulations yielded a HCl diffusion coefficient of $D = 5.1(\pm 1.6) \times 10^{-11}$ cm^2/s at $T = 189.4$ K.

B. Arrhenius Results for Diffusion of HCl Hydrates in Ice. The temperature dependence of the diffusion of HCl hydrates in ice was investigated to extract the diffusion kinetic parameters. An Arrhenius plot of the measured diffusion coefficients for $T = 169.0 - 194.9$ K is shown by the solid circles in Figure 7. The diffusion coefficients ranged from $D = 2.0(\pm 0.6) \times 10^{-13}$ cm^2/s at $T = 169.0$ K to $D = 1.1(\pm 0.2) \times 10^{-10}$ cm^2/s at $T = 194.9$ K. Arrhenius analysis of the diffusion coefficients yielded a diffusion activation energy of $E_A = 15.3 \pm 1.0$ kcal/mol and a diffusion preexponential of $D_o = 1.5 \times 10^{7\pm0.2}$ cm^2/s. The error limits were derived from a weighted least-squares linear regression of the diffusion data.

C. Results for Various Diffusion Times and HCl Exposures. LRD depth-profiling measurements of HCl hydrate diffusion in ice were performed over a wide range of diffusion times and initial HCl exposure conditions. The HCl diffusion times varied from $t = 120$ s to $t = 6300$ s, and the HCl exposures ranged from 6.0×10^{-5} Torr s to 1.8×10^{-3} Torr s. These experimental parameters were varied to investigate possible concentration effects on the measured HCl hydrate diffusion rates in ice.

Figure 8 shows the measured diffusion coefficients versus diffusion time at $T = 169.0$ K. The HCl diffusion coefficients in Figure 8 correspond to the spatial relaxation of a HCl trihydrate interlayer in an ice laminate at diffusion times ranging from $t = 600$ s to 6300 s. The diffusion coefficient of $D = 2.0 \times 10^{-13}$ cm^2/s was derived utilizing $2h$ and kAC_o values ranging from 0.01 to 0.50 μm and $2.0 \times 10^4 - 400$ μm^{-1}, respectively. These LRD results reveal that the measured HCl diffusion

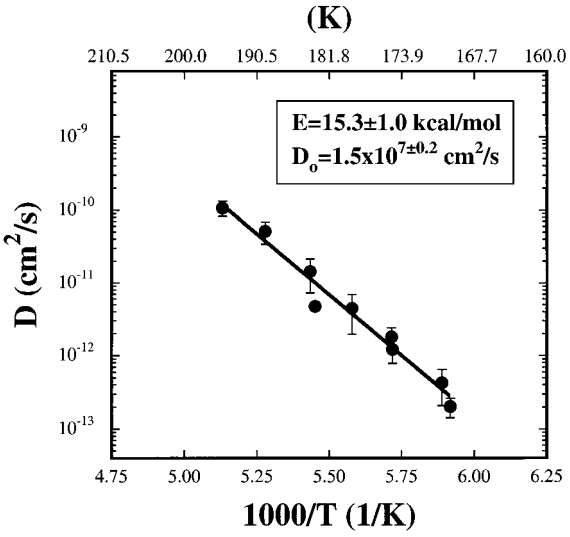

Figure 7. Arrhenius plot for HCl hydrate diffusion in crystalline ice measured using LRD depth-profiling. The kinetic parameters for HCl hydrate diffusion are $E_A = 15.3 \pm 1.0$ kcal/mol and $D_o = 1.5 \times 10^{7\pm0.2}$ cm^2/s.

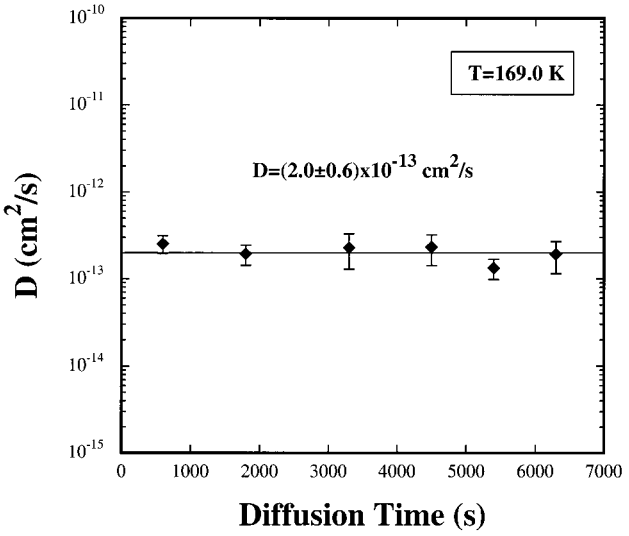

Figure 8. HCl hydrate diffusion coefficient measured at various diffusion times at $T = 169.0$ K. The solid line represents a diffusion coefficient of $D = 2.0 \times 10^{-13}$ cm^2/s.

coefficients were independent of diffusion time. The variation in the measured diffusion coefficients versus time was random and on the order of ~20%.

The measured HCl diffusion coefficients at $T = 169.0$ K and $T = 183.4$ K versus HCl exposure are displayed in Figure 9. The HCl diffusion coefficients at $T = 169.0$ K are represented by the solid diamonds. A diffusion coefficient of $2.0(\pm0.6) \times 10^{-13}$ cm^2/s was derived from LRD depth-profiling analysis at a diffusion time of $t = 1800$ s. The HCl diffusion coefficients at $T = 183.4$ K are denoted by the solid circles. A diffusion coefficient of $4.8(\pm0.5) \times 10^{-12}$ cm^2/s was determined from LRD depth-profiling analysis at a diffusion time of $t = 300$ s.

The LRD diffusion results shown in Figure 9 reveal that the measured HCl diffusion coefficients were independent of the initial HCl exposure. The diffusion coefficients only varied randomly by ~10−20% over a wide range of HCl exposures. Because the HCl exposure determines the HCl hydrate interlayer thickness, the HCl diffusion is independent of the initial HCl hydrate interlayer width.

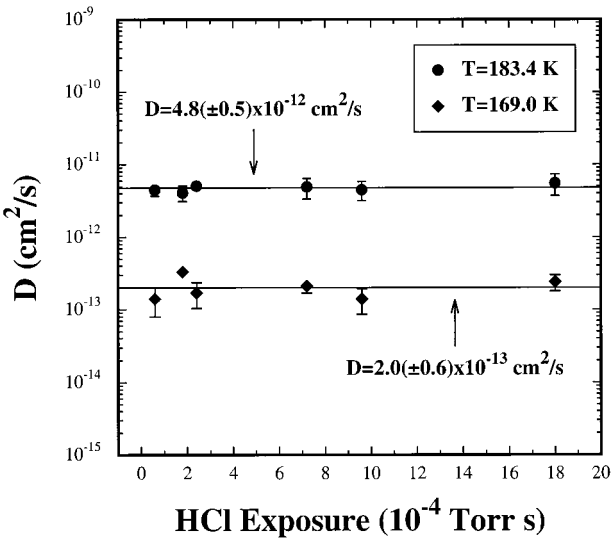

Figure 9. HCl hydrate diffusion coefficient versus initial HCl exposure. The HCl hydrate diffusion coefficients were derived after HCl diffusion at $T = 169.0$ K for $t = 1800$ s and after HCl diffusion at $T = 183.4$ K for $t = 300$ s.

IV. Discussion

A. Solubility of HCl in Ice Compared with HCl Concentration Measured by LRD Experiments. A variety of laboratory studies have measured HCl saturation solubilities in ice ranging from 1.3×10^{-7} to 1.8×10^{-4} mole fraction (~0.3 to 360 ppm by mass) over a temperature range from $T = 190-273$ K.[12,19−21,26,39−42] A very comprehensive recent examination of the equilibrium solubility of HCl in single-crystal ice has been performed using microtome sectioning and liquid chromatography.[12] Single-crystal ice samples were exposed to HCl partial pressures of 2.0×10^{-6} Torr to 3.0×10^{-5} Torr at $T = 238-265$ K for several weeks. After exposure and HCl diffusion, the HCl concentration versus distance in the ice sample was determined by the sequential removal of 25−50 μm ice layers via lathing followed by ion chromatography analysis for the chloride content of each ice layer. The equilibrium HCl mole fractions varied from 1.24×10^{-6} to 12.36×10^{-6} (2.48−24.72 ppm by mass) over the temperature range from 238 to 265 K.[12]

Earlier radioactive tracer experiments using H^{36}Cl revealed a small but finite solubility of HCl in crystalline ice.[21] The HCl equilibrium solubility values were independent of temperature over the range $T = 255-269$ K and varied from 1.25×10^{-7} mole fraction (0.25 ppm by mass) to 1.43×10^{-7} mole fraction (0.29 ppm by mass). Additional HCl solubility measurements in ice were conducted using a scanning electron microscope equipped with an energy-dispersive X-ray microanalysis system.[26] The X-ray experiments determined a HCl saturation solubility of $< 1.8 \times 10^{-4}$ mole fraction (360 ppm by mass) at $T = 198$ K.

The detection limit for the microtome sectioning technique coupled with ion chromatography analysis is $\sim 1 \times 10^{-8}$ HCl mole fraction or ~20 ppb HCl by mass. In comparison, the LRD technique combined with quadrupole mass spectrometry provides a detection limit of $\sim 2 \times 10^{-6}$ HCl mole fraction or ~4 ppm HCl by mass. This LRD detection limit corresponds to an elliptical ice desorption area of ~175 μm × ~225 μm and a desorption depth of ~1 μm. Consequently, the sensitivity of the microtome sectioning technique exceeds the LRD sensitivity by a factor of ~200. The sensitivity of the LRD technique is insufficient to measure the diffusion of HCl

TABLE 1: HCl Diffusion Coefficients in Ice Measured Using Various Experimental Techniques

experimental technique	HCl diffusion coefficient (cm^2/s)	diffusion temperature (K)	HCl concentration (mole fraction)	reference
radioactive tracer liquid scintillation	$2.2 \times 10^{-8}-1.6 \times 10^{-7}$	255−269	$(1.25-1.43) \times 10^{-7}$	21
microtome sectioning/IC	$4.0 \times 10^{-12}-7.2 \times 10^{-12}$	238−265	$(1.24-12.36) \times 10^{-6}$	12,19,20
NMR spin−lattice relaxation	$\sim 4 \times 10^{-9}$	258	$\sim 1 \times 10^{-4}$	23
SEM/X-ray microanalysis	$< 1 \times 10^{-13}$	253	$< 1.8 \times 10^{-4}$	26
LRD depth-profiling	$2.0(\pm 0.6) \times 10^{-13}$ to $1.1(\pm 0.2) \times 10^{-10}$	169.0−194.9	$< 1 \times 10^{-3}-0.01$	this study
flow reactor	$\sim 2 \times 10^{-13}$	188	$(0.33-6.3) \times 10^{-4}$	25
spectrophotometric (Hg lamp)	$\sim 1 \times 10^{5}$	185	$(0.3-1.0) \times 10^{-2}$	8
FT-IR spectroscopy	$(\sim 2-3) \times 10^{-12}$	158	~0.02−0.14	24
ATR−IR spectroscopy	$\sim 1 \times 10^{-11}$	150	~0.02−0.14[a]	22

[a] HCl concentration not cited in original reference. HCl concentration values were estimated from HCl exposure conditions.

impurities in ice at concentrations of $\leq 1 \times 10^{-6}$ mole fraction (≤ 2 ppm by mass).

Calibrated HCl LRD signals near the center of the spatial distributions in Figures 5 and 6 correspond to HCl levels of $\sim(5-8) \times 10^8$ molecules/μm^3 or ~0.01−0.02 HCl mole fraction. The HCl concentrations in the low intensity wings of the measured spatial distributions are typically ≤10% of the maximum HCl concentration and correspond to HCl levels of $\leq 1 \times 10^{-3}$ mole fraction. Consequently, the HCl concentrations measured by these LRD HCl hydrate diffusion studies are a factor of ≤80 to $\sim 1 \times 10^4$ times larger than the HCl equilibrium saturation solubilities. The HCl diffusion kinetics measured by these LRD depth-profiling studies do not correspond to HCl impurity level diffusion near the solubility limit. Rather, the LRD HCl diffusion experiments have monitored the migration of HCl hydrates in ice.

The HCl molecules were contained initially in a region with a local H_2O:HCl stoichiometry of 3:1 corresponding to a HCl trihydrate phase with a thickness of ~0.1 μm.[36] HCl diffusion from this trihydrate phase involves the migration and dilution of various HCl hydrate phases through the ice lattice. Numerous studies exist concerning the formation and identification of amorphous and crystalline HCl hydrates in ice.[24,36,43−46] Amorphous HCl-ice hydrate thin films with various H_2O:HCl stoichiometries have been observed using infrared (IR) spectroscopy.[24,43,44] IR spectroscopy and laser-induced thermal desorption (LITD) techniques have also been utilized to assign the various mono-, di-, tri-, tetra-, and hexa-hydrate phases of crystalline HCl hydrates in ice over the temperature range from $T = 85-215$ K.[24,36,43−46] Numerous studies have also been conducted to define the various hydrates on the HCl/ice phase diagram.[12,47,48]

B. Comparison Between HCl Hydrate Diffusion and Previous Measurements of HCl Diffusion in Ice. HCl diffusion in ice has been investigated using a variety of direct experimental techniques including microtome sectioning and liquid chromatography,[12,19,20] radioactive tracer methods,[21] scanning electron microscopy (SEM) and X-ray analysis,[26] and attenuated total internal reflection infrared (ATR−IR) spectroscopy.[22] The HCl diffusion coefficients in ice measured using various experimental techniques are summarized in Table 1. Conflicting HCl diffusion kinetics have been measured with reported HCl diffusion coefficients ranging from $D \approx 10^{-5}$ cm^2/s to $D \approx 10^{-13}$ cm^2/s at $T \approx 185$ K.[1,8,12,19−25] The large variability may be caused by the wide range of experimental conditions and techniques utilized in the HCl diffusion measurements. The various HCl exposure conditions and HCl concentrations, as well as different ice growth conditions, ice morphologies, and spatial resolutions and detection sensitivities may have influenced the HCl diffusion measurements.

The microtome and chromatography experiments measured HCl diffusion in laboratory grown single-crystal ice over the temperature range from $T = 238-265$ K.[12,19,20] Following HCl exposure and HCl diffusion, the diffusion profiles yielded HCl diffusion coefficients ranging from $D = 4.0 \times 10^{-12}$ cm^2/s at $T = 238$ K to $D = 7.2 \times 10^{-12}$ cm^2/s at $T = 265$ K.[12,19,20] These studies suggested that the HCl diffusion measurements were influenced by short circuits caused by small angle boundaries in the single-crystal ice samples. Because the diffusion rate is enhanced significantly by the presence of short circuits, the measured HCl diffusion coefficients represent only upper limits. The variation in the density of small angle boundaries and defects caused appreciable scatter in the measured diffusion coefficients. The uncertainty in the diffusion coefficients precluded Arrhenius analysis and determination of the HCl diffusion kinetic parameters.

The microtome sectioning diffusion experiments measured HCl impurity diffusion in ice at HCl levels near the solubility limit at HCl mole fractions of 1.24×10^{-6} to 12.36×10^{-6}.[12] The HCl LRD kinetic results for HCl hydrate diffusion can be extrapolated to the higher temperatures of the microtome sectioning experiments. These extrapolations predict diffusion coefficients ranging from $D = 1.3 \times 10^{-7}$ cm^2/s at $T = 238$ K to $D = 3.6 \times 10^{-6}$ cm^2/s at $T = 265$ K. These LRD HCl hydrate diffusion coefficients are $\sim 3 \times 10^4$ to $\sim 5 \times 10^5$ times larger than the HCl impurity diffusion coefficients measured using microtome analysis. This large difference may be attributed to the difference between HCl impurity and HCl hydrate diffusion. In addition, HCl hydrates at higher temperatures may have different thermodynamic phases than HCl hydrates at the lower temperatures used in the LRD diffusion experiments.

An earlier study of HCl impurity diffusion in ice used radioactive tracer and liquid scintillation spectrometric techniques.[21] The tracer experiments measured the $H^{36}Cl$ content versus depth in single-crystal ice specimens exposed to frozen HCl-saturated polycrystalline ice disks. Analysis of the $H^{36}Cl$ tracer diffusion profiles yielded HCl diffusion coefficients ranging from $D = 2.2 \times 10^{-8}$ cm^2/s at $T = 255$ K to $D = 1.6$

$\times 10^{-7}$ cm^2/s at $T = 269$ K. These diffusion coefficients are also much larger than the more recent microtome measurements. Reanalysis of the temperature dependence of the $H^{36}Cl$ tracer diffusion coefficients yields an HCl diffusion activation barrier of $E = 19.3$ kcal/mol and a diffusion preexponential of $D_o = 6.86 \times 10^8$ cm^2/s.

The location and migration of HCl in frozen HCl−H_2O aqueous solutions were also studied using a scanning electron microscope (SEM) equipped with an energy-dispersive X-ray microanalysis system.[26] Sub-molar HCl aqueous solutions were fast-frozen to generate polycrystalline ice samples consisting of ice crystals ∼10−100 μm in diameter. X-ray analysis demonstrated that HCl was preferentially located at triple junctions with very low X-ray counts for Cl in adjacent two-grain boundaries.[26] HCl diffusion coefficients were derived by monitoring the HCl concentration versus distance from the triple junction HCl source. The SEM and X-ray results showed very low HCl mobility in the ice lattice with an upper limit for the HCl diffusion coefficient of $D < 10^{-13}$ cm^2/s at $T = 253$ K. This HCl impurity diffusion coefficient is smaller than the diffusion coefficients measured by the microtome or radioactive tracer studies.

More recent experiments have measured HCl diffusion at much higher concentrations in the HCl hydrate regime. Attenuated total internal reflection infrared (ATR−IR) spectroscopy has been applied recently to examine HCl diffusion in ice.[22] The diffusion rate of the ionized HCl hydrate of the form $(H_2O)_nH_3O^+Cl^-$ was determined by monitoring the growth of the hydrogen-bonded ν_{OH} band of the hydroxonium ion (H_3O^+) versus time following HCl exposure. The diffusion coefficient for the $(H_2O)_nH_3O^+Cl^-$ species was measured to be $D \approx 1 \times 10^{-11}$ cm^2/s at 150 K. In comparison, an extrapolation of the HCl LRD kinetic results to lower temperatures yields a HCl diffusion coefficient of $D = 7.7 \times 10^{-16}$ cm^2/s at 150 K. The much larger HCl diffusion coefficient derived from the ATR−IR experiments may be explained by grain boundaries and defects in the ice film that was grown by H_2O vapor deposition on a Ge internal reflection element at 140 K.

Estimates of the HCl diffusion coefficient in ice have also been inferred from FTIR spectroscopy studies.[24] The FTIR diffusion experiments monitored the uptake of HCl on water-ice films ∼0.3 μm to 5.7 μm in thickness and followed the conversion of the ice film to a stable HCl-hydrate phase. A rough estimate of the HCl diffusion coefficient can be obtained from the FTIR data by determining the time required to convert an ice film of known thickness. For HCl uptake on a ∼0.3 μm ice film, ∼3.5 min was required for complete conversion to the HCl hexahydrate and corresponds to a HCl diffusion coefficient of $\sim 2 \times 10^{-12}$ cm^2/s at $T = 158$ K. Experiments with thicker ice films over longer time intervals yielded a similar estimate of the HCl diffusion coefficient of $\sim 3 \times 10^{-12}$ cm^2/s at $T = 158$ K.[24]

The HCl diffusion coefficients of $\sim 2 \times 10^{-12}$ cm^2/s derived indirectly from the FTIR measurements on HCl-hydrate films at 158 K are much larger than the HCl diffusion coefficient of $D = 1.0 \times 10^{-14}$ cm^2/s at 158 K obtained by extrapolation of the HCl LRD kinetic results. The larger HCl diffusion rate observed in the FTIR experiments may be due to the ice film preparation conditions. Micron-sized ice films were grown by backfill H_2O vapor deposition on a silicon substrate at 155 K.[24] The polycrystalline film results in the formation of dislocations and grain boundaries in the ice samples that may have facilitated the HCl diffusion.

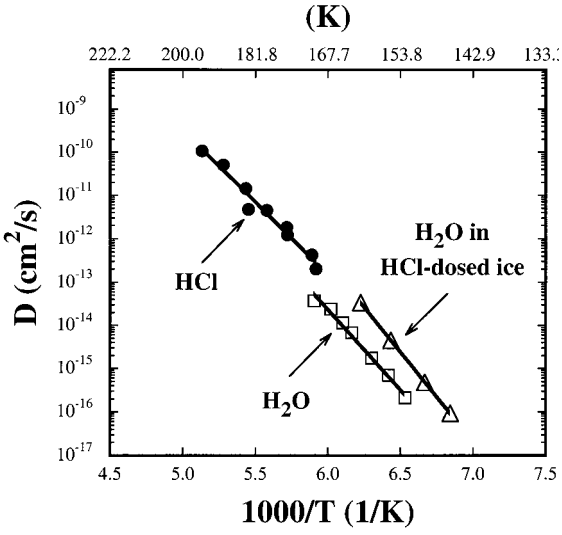

Figure 10. Arrhenius plots for HCl diffusion in pure ice measured using LRD depth-profiling (this study) and H_2O diffusion in pure and HCl-dosed single-crystal ice multilayers measured using LITD isothermal desorption depth-profiling (ref 37, 54 and 55).

The large range of results for HCl diffusion in ice is attributed to both the HCl concentrations and the nature of the ice samples. At high HCl concentrations, HCl hydrate diffusion may have a much larger diffusion coefficient than HCl impurities in ice at low HCl concentrations. Ice samples with more grain boundaries and defects may also display much larger HCl diffusion coefficients than single-crystal ice samples. The HCl concentrations and characteristics of the ice samples must be clearly defined to compare the various HCl diffusion measurements.

C. Mechanism of HCl Hydrate Diffusion. Studies regarding the mechanism of diffusion in ice are virtually nonexistent. Isotope tracer,[49,50] X-ray topography[51,52] and LITD isothermal desorption depth-profiling[5,29,37,53−55] techniques have been applied to examine H_2O self-diffusion kinetics in crystalline and polycrystalline ice over the temperature range from $T = 145-273$ K. These previous experiments have demonstrated that the diffusion coefficients and diffusion activation energies for D_2O ($^2H_2{}^{16}O$), T_2O ($^3H_2{}^{16}O$), $H_2{}^{18}O$ and HDO in ice are approximately equivalent.[29,37,49,50,53] The close similarity of the diffusion kinetics for the HDO and $H_2{}^{18}O$ isotopes argues for a molecular transport mechanism.[37,49,50,53]

The issue of whether H_2O diffusion in ice occurs via a vacancy- or interstitial-mediated mechanism is less clear and currently unresolved.[49,50] X-ray topography studies on the growth processes associated with dislocation loops and dipoles revealed that the predominant point defects in ice are self-interstitials at temperatures exceeding 223 K.[51,52] Consequently, H_2O self-diffusion is tentatively believed to occur by a interstitial-mediated mechanism for $T > 223$ K and by a vacancy-mediated mechanism for $T < 223$ K.[51,52]

A comparison of the LRD results for HCl hydrate diffusion with previously measured H_2O diffusion kinetics may provide insight into the mechanism of HCl hydrate diffusion in ice. Figure 10 shows the HCl hydrate diffusion coefficients (solid circles) along with the diffusion coefficients for H_2O migration in pure and HCl-dosed single-crystal ice multilayers.[37,54,55] The H_2O diffusion coefficients in pure and acid-dosed ice multilayers were measured previously using laser-induced thermal desorption (LITD) probing and isothermal desorption depth-profiling techniques.[37,54,55]

An Arrhenius plot of the measured H_2O diffusion coefficients in pure single-crystal ice multilayers for $T = 153.2-170.0$ K

is shown by the open squares in Figure 10. For pure ice multilayers, the H_2O diffusion coefficients ranged from $D = 2.2(\pm0.3) \times 10^{-16}$ cm^2/s at $T = 153.2$ K to $D = 4.4(\pm0.4) \times 10^{-14}$ cm^2/s at $T = 170.0$ K.[37,54] Arrhenius analysis of the temperature-dependent H_2O diffusion coefficients into pure ice yielded a diffusion activation energy of $E_A = 17.0 \pm 1.0$ kcal/mol and a diffusion preexponential of $D_o = 4.2 \times 10^{8\pm0.1}$ cm^2/s.[37,54]

The Arrhenius diffusion data for H_2O diffusion into crystalline ice multilayers exposed to HCl are denoted by the open triangles in Figure 10. The diffusion coefficients for H_2O diffusion into HCl-dosed crystalline ice films were ~10−20 times larger than the H_2O diffusion coefficients into pure ice and ranged from $D = 9.8(\pm1.1) \times 10^{-17}$ cm^2/s at $T = 146.2$ K to $D = 3.5(\pm0.4) \times 10^{-14}$ cm^2/s at $T = 160.7$ K.[54,55] The diffusion kinetic parameters for H_2O diffusion into HCl-dosed crystalline ice films were $E_A = 19.0 \pm 0.3$ kcal/mol and $D_o = 2.4 \times 10^{12\pm0.02}$ cm^2/s.[54,55]

An extrapolation of the H_2O diffusion coefficients would overlap with the diffusion coefficients for the HCl hydrate diffusion. The similarity between these diffusion kinetics suggests that HCl hydrate diffusion in ice may be controlled by H_2O diffusion. At the temperatures displayed in Figure 10, H_2O diffusion may be controlled by a vacancy-mediated diffusion mechanism.[51] Consequently, the diffusion and dilution of HCl hydrates in ice may be controlled by H_2O vacancy diffusion. H_2O vacancies may be required to diffuse to sites adjacent to H_3O^+ and Cl^- species prior to their movement into these vacancy sites.

The dependence of HCl hydrate diffusion on H_2O vacancies is appealing because the measured HCl hydrate diffusion is independent of HCl concentration and the thickness of the initial HCl hydrate interlayer. As HCl in the initial HCl trihydrate diffuses and is diluted in the ice lattice, the stoichiometry of the HCl hydrate would change progressively from trihydrate to tetrahydrate to hexahydrate. The concentration independence of HCl hydrate diffusion argues that the HCl concentration cannot control the diffusion mechanism. The H_2O vacancies may display diffusion kinetics that are not significantly affected by the H_3O^+ and Cl^- species in ice. The similar diffusion kinetics for H_2O diffusion in pure and HCl-dosed ice are in general agreement with this suggestion.

V. Conclusions

HCl hydrate diffusion kinetics in ice were measured using novel infrared laser resonant desorption (LRD) depth-profiling techniques. These new LRD methods facilitate quantitative depth-profiling and real time diffusion measurements in ice films with submicron spatial resolution and high sensitivity. The HCl hydrate diffusion coefficients measured using LRD ranged from $D = 2.0(\pm0.6) \times 10^{-13}$ cm^2/s at $T = 169.0$ K to $D = 1.1(\pm0.2) \times 10^{-10}$ cm^2/s at $T = 194.9$ K. Arrhenius analysis of the diffusion rates yielded a diffusion activation energy of $E_A = 15.3 \pm 1.0$ kcal/mol and a diffusion preexponential of $D_o = 1.5 \times 10^{7\pm0.2}$ cm^2/s. The HCl diffusion coefficients were independent of the total diffusion time and the initial HCl exposure conditions used to prepare the HCl hydrates.

Extrapolation of the HCl hydrate diffusion coefficients to higher temperatures reveals that the HCl hydrate diffusion is much faster than HCl impurity diffusion in ice measured using microtome sectioning and scanning electron microscope experiments. The extrapolated HCl hydrate diffusion coefficients are also much lower than HCl diffusion rates measured using infrared methods on polycrystalline films. These comparisons suggest that HCl hydrate diffusion is much faster than HCl impurity diffusion and that polycrystalline ice films display much larger diffusion coefficients than single-crystal films. The HCl hydrate diffusion rates are similar to H_2O diffusion rates in pure and HCl-dosed crystalline ice multilayers. The correlation between the HCl hydrate diffusion kinetics and H_2O diffusion kinetics suggests that HCl hydrate diffusion and dilution in the ice lattice may be governed by a H_2O vacancy-mediated diffusion mechanism.

Acknowledgment. The authors gratefully acknowledge the financial support of the National Science Foundation under Grant No. CHE-9905812.

References and Notes

(1) Wolff, E. W.; Bales, R. C. *Chemical Exchange Between the Atmosphere and Polar Snow*; Springer-Verlag: Berlin, 1996.
(2) Legrand, M.; Mayewski, P. *Rev. Geophys.* **1997**, *35*, 219.
(3) Delmas, R. J.; Legrand, M. *The Environmental Record in Glaciers and Ice Sheets Dahlem Workshop Report*; Oeschger, H., Langway, C. C., Eds.; Wiley and Sons: Chichester, U. K., 1989.
(4) Pasteur, E. C.; Mulvaney, R. *J. Geophys. Res.* **2000**, *105*, 11.
(5) George, S. M.; Livingston, F. E. *Surf. Rev. and Lett.* **1997**, *4*, 771.
(6) Tabazadeh, A.; Turco, R. P. *J. Geophys. Res.* **1993**, *98*, 12727.
(7) Turco, R. P.; Toon, O. B.; Hamill, P. *J. Geophys. Res.* **1989**, *94*, 16493.
(8) Molina, M. J.; Tso, T. L.; Molina, L. T.; Wang, F. C. Y. *Science* **1987**, *238*, 1253.
(9) Tolbert, M. A.; Rossi, M. J.; Malhotra, R.; Golden, D. M. *Science* **1987**, *238*, 1258.
(10) Hanson, D. R.; Ravishankara, A. R. *J. Geophys. Res.* **1991**, *96*, 5081.
(11) Solomon, S. *Rev. Geophys.* **1988**, *26*, 131.
(12) Thibert, E.; Domine, F. *J. Phys. Chem. B* **1997**, *101*, 3554.
(13) Borrmann, S.; Solomon, S.; Dye, J. E.; Luo, B. *Geophys. Res. Lett.* **1996**, *23*, 2133.
(14) Jensen, E. J.; Toon, O. B.; Selkirk, H. B.; Spinhirne, J. D.; Schoeberl, M. R. *J. Geophys. Res.* **1996**, *101*, 21 361.
(15) Zondlo, M. A.; Barone, S. B.; Tolbert, M. A. *Geophys. Res. Lett.* **1997**, *24*, 1391.
(16) Stephens, G. L.; Tsay, S.-C.; Stackhouse, J. P. W.; Flatau, P. J. *J. Atmos. Sci.* **1990**, *47*, 1742.
(17) Ackerman, T. P.; Liou, K.-N.; Valero, F. P. J.; Pfister, L. *J. Atmos. Sci.* **1988**, *45*, 1606.
(18) Domine, F.; Thibert, E.; Van Landeghem, F.; Silvente, E.; Wagnon, P. *Geophys. Res. Lett.* **1994**, *21*, 601.
(19) Domine, F.; Thibert, E. *Geophys. Res. Lett.* **1996**, *23*, 3627.
(20) Domine, F.; Thibert, E.; Silvente, E.; Legrand, M.; Jaffrezo, J.-L. *J. Atmos. Chem.* **1995**, *21*, 165.
(21) Krishnan, P. N.; Salomon, R. E. *J. Phys. Chem.* **1969**, *73*, 2680.
(22) Horn, A. B.; Sully, J. *J. Chem. Soc., Faraday Trans.* **1997**, *93*, 2741.
(23) Barnaal, D.; Slotfeldt-Ellingsen, D. *J. Phys. Chem.* **1983**, *87*, 4321.
(24) Koehler, B. G.; McNeill, L. S.; Middlebrook, A. M.; Tolbert, M. A. *J. Geophys. Res.* **1993**, *98*, 10 563.
(25) Chu, L. T.; Leu, M.-T.; Keyser, L. F. *J. Phys. Chem.* **1993**, *97*, 7779.
(26) Wolff, E. W.; Mulvaney, R.; Oates, K. *Geophys. Res. Lett.* **1989**, *16*, 487.
(27) Livingston, F. E.; Smith, J. A.; George, S. M. *Analytical Chem.* **2000**, *72*, 5590.
(28) Krasnopoler, A.; George, S. M. *J. Phys. Chem. B* **1998**, *102*, 788.
(29) Brown, D. E.; George, S. M. *J. Phys. Chem.* **1996**, *100*, 15 460.
(30) Mak, C. H.; Brand, J. L.; Deckert, A. A.; George, S. M. *J. Chem. Phys.* **1986**, *85*, 1676.
(31) George, S. M. *J. Vac. Sci. Technol. A* **1986**, *4(5)*, 2394.
(32) Deckert, A. A.; Brand, J. L.; Arena, M. V.; George, S. M. *Surf. Sci.* **1989**, *208*, 441.
(33) Toon, O. B.; Tolbert, M. A.; Koehler, B. G.; Middlebrook, A. M.; Jordan, J. *J. Geophys. Res.* **1994**, *99*, 25.
(34) George, S. M.; DeSantolo, A. M.; Hall, R. B. *Surf. Sci.* **1985**, *159*, L425.
(35) Haynes, D. R.; Tro, N. J.; George, S. M. *J. Phys. Chem.* **1992**, *96(21)*, 8502.

(36) Foster, K. L.; Tolbert, M. A.; George, S. M. *J. Phys. Chem.* **1997**, *101*, 4979.
(37) Livingston, F. E.; Whipple, G. C.; George, S. M. *J. Chem. Phys.* **1998**, *108*, 2197.
(38) Crank, J. *The Mathematics of Diffusion*, 2nd ed.; Clarendon Press: Oxford, U. K., 1975.
(39) Hanson, M.; Mauersberger, K. *Geophys. Res. Lett.* **1988**, *15*, 1507.
(40) Hanson, D. R.; Mauersberger, K. *J. Phys. Chem.* **1990**, *94*, 4700.
(41) Gross, G. W.; Wong, P. W.; Humes, K. J. *J. Chem. Phys.* **1977**, *67*, 5264.
(42) Seidensticker, R. G. *J. Chem. Phys.* **1972**, *56*, 2853.
(43) Delzeit, L.; Rowland, B.; Devlin, J. P. *J. Phys. Chem.* **1993**, *97*, 10 312.
(44) Ritzhaupt, G.; Devlin, J. P. *J. Phys. Chem.* **1991**, *95*, 90.
(45) Abbatt, J. P.; Beyer, K. D.; Fucaloro, A. F.; McMahon, J. R.; Woolridge, P. J.; Zhang, R.; Molina, M. J. *J. Geophys. Res.* **1992**, *97*, 15 819.
(46) Gilbert, A. S.; Sheppard, N. *J. Chem. Faraday Trans. 2* **1973**, *69*, 1628.
(47) Molina, M. J. The Probable Role of Stratospheric "Ice" Clouds: Heterogeneous Chemistry of the "Ozone Hole". In *The Chemistry of the Atmosphere: Its Impact on Global Change*; Calvert, J. G., Ed.; Blackwell Scientific: Boston, MA, 1994.
(48) Wooldridge, P. J.; Zhang, R.; Molina, M. J. *J. Geophys. Res.* **1995**, *100*, 1389.
(49) Hobbs, P. V. *Ice Physics*; Clarendon Press: Oxford, U. K., 1974.
(50) Petrenko, V. F.; Whitworth, R. W. *Physics of Ice*; Oxford University Press: New York, 1999.
(51) Goto, K.; Hondoh, T.; Higashi, A. *Jpn. J. Appl. Phys.* **1986**, *25*, 351.
(52) Hondoh, T.; Goto, A.; Hoshi, R.; Ono, T.; Anzai, H.; Kawase, R.; Pimienta, P.; Mae, S. *Rev. Sci. Instrum.* **1989**, *60(7)*, 2494.
(53) Livingston, F. E.; Whipple, G. C.; George, S. M. *J. Phys. Chem.* **1997**, *101*, 6127.
(54) Livingston, F. E.; George, S. M. *Defect and Diffus. Forum* **1998**, *160*−*161*, 25.
(55) Livingston, F. E.; George, S. M. *J. Phys. Chem. B* **1999**, *103*, 4366.